Granular flow on asteroids using DEM in LAMMPS

Deepayan Banik

August 2019

1 Literature survey

- A rubble-pile asteroid is one which is composed of several particles rather than being a single piece of rock. One of the interesting surface phenomena observed on such objects is the apparent sorting of surface material like that seen on Itokawa, visited by the Japanese spacecraft, Hayabusa 1. Bigger rocks are seen on 'hills' and smaller ones in 'valleys'. Here 'hills' and 'valleys' have to be understood in the context of the effective gravitational potential of a small, self-gravitating, irregular, rotating body [19]. Recently NASA's OSIRIS-REx have reported mass ejection from the surface of asteroid Bennu due to the combined effect of rotation and a weak gravitational field, causing material to orbit the central body. Some of these have been observed to rain down on the surface resulting in redistribution of surface mass [20]. These make the surface mechanics of such objects an interesting thing to study.
- Let us have a glimpse into the history of theoretical studies on asteroids.
- Chandrasekhar (1969) in [1] talked about the study of gravitational equilibrium of rotating masses being started by Newton, as early as late 17th century, followed up by Maclaurin, Jacobi and several other scientists. The primary aspects of these studies included eccentricity, rotation, effects of tidal forces and stability of equilibrium shapes.
- Darwin (1906) [2], probed the existence of equilibrium shapes for two cases. First, when the liquid satellite was in a gravitational field much stronger than it's own. Two, when it was entangled with another one of similar mass and orientation.
- In a series of work presented in the *Astrophysical Journal* (vols. 134-57) Lebovitz and Chandrasekhar have explored a significant portion of the deformation dynamics and equilibriation of ellipsoids using the *virial method*, which in essence, is an application of the method of moments to the hydrodynamical equations that govern the movement of fluids in a self-gravitating environment.
- Forays into solid satellites were made by Aggarwal *et. al.* [5] (1974), Dobrovolskis (1982, 1990) [6] and Davidsson (2001) [7], where linear elasticity was coupled with a failure criterion to judge the survival of the satellite in different environments.
- The above analyses do not work for rubble piles.
- Granular aggregates held together only by self gravity are called rubble piles. They cannot sustain any tensile stress, if cohesionless, but inter-grain friction allows sustenance of a finite amount of shear stress. This is why we may walk on sand but not on water. For the same reason, Sharma (2019) suggests that, equilibrium shapes of rubble piles will be different from those that have a solid coherent core, with grains strewn over the surface in a shallow layer [4] compared to completely granular aggregates having cohesion.

- Holsapple and Michel (2006, 2008) considered spherical central bodies and symmetric satellites, so as to avoid tidal torques and products of inertia. Sharma [3] in 2009 and 2010 revisited Darwin's work [2] for granular satellites modelling them as cohesionless, rigid plastic substances with a Drucker–Prager yield criterion, using volume averaging techniques based on the *virial method*. He addressed oblate central objects, restricting the satellite to symmetric orientations.

- As such, asymmetries have not be explored in all it's extent. We venture into the most basic axial asymmetry in 2 dimensions, i.e. an ellipse.

- Let is look into the history of ellipsoidal approximations to asteroids and their simulations.

- Chauvineau *et. al.*(1993) [8] and Scheeres (1994) [9] talked about orbital dynamics of particles around triaxial ellipsoids. Guibout and Scheeres (2003) [10] spoke about linear stability of equilibrium points located on ellipsoids and analysed zero-velocity curves on their surface.

- One of the earliest attempts at DEM using hard spheres made by Walsh *et. al.* (2008) [11] which showed that an asteroid with a rigid core and loose granular layer on the surface sheds mass to form binary systems due to rotational instability.

- In 2012 [12] Sanchez and Scheeres used a SSDEM model with self-gravity to study reshaping phenomena of rubble piles with varied rotation rates and tried to match the results with the theory of Holsapple. They have talked about critical angular velocity required for reshaping based on inter-particle friction. All this was, however, for a completely deforming asteroid without any rigid parts. A DEM code called PKDgrav was used, where all particles had two ways of interacting with one another. One, collisions modelled using tangential and normal springs and dashpots. Two, mutual gravitational attraction.

- Mass loss and satellite formation from rubble piles with variable core sizes were studied in 2012 by Walsh *et. al.* [13] under the action of slow spin up due to YORP for angles of friction ranging from 0^o to 40^o. Pravec *et. al.* (2007) [23] states that critical shedding Ω, for asteroid having length of the order of hundred meters, has been observed to be $\sim 7.5 \times 10^{-4} rads^{-1}$.

- The increase in structural strength of asteroids with density of the core was observed by Hirabayashi (2014) [14] using a two-bulk-density-layer model. Further, plastic finite element analysis was performed by Hirabayashi and Scheeres (2015) [15] to understand the failure mode of asteroid (29075) 1950 DA, concluding the disruption of it's core. From these, Hirabayashi *et. al.* gathered that interior strength must be higher for surface failure to happen at high rotation rates and thus they model their asteroid as a spherical shell on an internal core having different cohesive strengths [16]. This is why we have decided to go ahead with a non-deforming core with material flowing on the surface.

- We are concerned with shallow granular flows over the two dimensional, elliptic, equatorial bed of rotating and gravitating asteroids. We would like to study the effects of spin-up of the rigid core, due to YORP or tidal forces, on uniform surface topographies and run-out distances of avalanches due to hill-breaks resulting from probable internal tremors or thermal fragmentation. In our study we identify a few regimes of angular velocities corresponding to surface deformation and mass shedding. A similar kind of classification has been mentioned in [16], which says that at a lower bound, the granular aggregate should not fail structurally, but, at an upper bound, it does. Beyond an angular velocity higher than the upper bound, there is mass shedding.

- We study values of inter-particle friction, in the range of angle of friction 0° to 15°, even though this a slab lower than what it actually should be. This allows us to capture all

dynamical regimes since higher angles restrict movement in lower superficial geopotentials. However, this range is not unnatural keeping in mind the fluidization of regolith caused by impact-induced seismic shaking as mentioned by Krohn *et al.* (2014)[26] and Mudhroch *et al.* (2015)[17], which reduces effective angle of friction.

2 Simulation methodology

We are interested in a global simulation for shallow flow of granular material over an ellipse under the influence of it's rotation and gravitational field. This way of modelling an asteroid is different from the ones done previously by Walsh *et. al.* using HSDEM (2008) [11], Sanchez and Scheeres using SSDEM (2012) [12] since we use an elliptic gravity field for the core and the grains flowing over it interact with one another only via. collisions. The shallow layer approximation allows us to neglect the gravitational field due to the particles as compared to the solid elliptical core. Modelling asteroids as complete granular aggregates requires considerable computational effort, whereas, this method reduces expenses drastically. However, the drawback is that, since the flowing particles do not have any self-gravity, some interesting post shedding phenomena, like binary formation [11], etc. are not accurately captured.

2.1 3D formula for the gravitational potential in the exterior of a triaxial ellipsoid

Consider a constant density ellipsoid with semi-major axes $\gamma \leq \beta \leq \alpha$ normalized by any length, say L, of the order of the semi-major axis of the ellipsoid. The shape is defined by the equation $(x/\alpha)^2 + (y/\beta)^2 + (z/\gamma)^2 \leq 1$. The total mass of a constant density ellipsoid is $M = \frac{4\pi}{3}\sigma\alpha\beta\gamma$ and $\mu = GM$. The potential is,

$$U(\mathbf{r}) = -\frac{3\mu}{4}\int_{\lambda(\mathbf{r})}^{\infty} \Phi(\mathbf{r}, u)\frac{du}{\Delta(u)}$$

where,

$$\Phi(\mathbf{r}, u) = \frac{x^2}{\alpha^2+u} + \frac{y^2}{\beta^2+u} + \frac{z^2}{\gamma^2+u} - 1 \quad and \quad \Delta(u) = \sqrt{(\alpha^2+u)(\beta^2+u)(\gamma^2+u)}$$

$\lambda(\mathbf{r})$ is defined by the equation $\phi(\mathbf{r}, \lambda) = 0$. This equation is equivalent to a cubic polynomial and λ is defined to be the maximum real root, which will always exist. The position vector $\mathbf{r}$ is specified in the principal axis frame with the x-axis along the long axis α, y along the intermediate axis β, and z along the short axis γ. The cubic is,

$$\lambda^3 + p\lambda u^2 + q\lambda u + r = 0$$

The normalized coordinates of the point at which the potential has to be found is (x_p, y_p, z_p). The GSL fucntion *gsl-poly-solve-cubic* is used to solve this, where,

$$p = \alpha^2 + \beta^2 + \gamma^2 - x_p^2 + y_p^2 + z_p^2$$

$$q = \sum(\alpha^2\beta^2 - (\alpha^2+\beta^2)z_p^2)$$

$$r = \alpha^2\beta^2\gamma^2 - \sum(\alpha^2\beta^2 z_p^2)$$

For the evaluation of the elliptic integral, Carlson's symmetric basis of functions are used. The GSL functions *gsl-sf-ellint-RD/RF* that calculate the following serve the purpose,

$$RD(x, y, z) = \frac{3}{2}\int_0^{\infty} \frac{dt}{\sqrt{(t+x)(t+y)(t+z)^2}}$$

$$RF(x,y,z) = \frac{1}{2}\int_0^\infty \frac{dt}{\sqrt{(t+x)(t+y)(t+z)}}$$

$U(\mathbf{r})$ is given by the following proceedure:

$$V_1 = \frac{2}{3}\alpha\beta\gamma \;\; x_p^2 \;\; RD(\beta^2+\lambda, \gamma^2+\lambda, \alpha^2+\lambda)$$

$$V_2 = \frac{2}{3}\alpha\beta\gamma \;\; y_p^2 \;\; RD(\gamma^2+\lambda, \alpha^2+\lambda, \beta^2+\lambda)$$

$$V_3 = \frac{2}{3}\alpha\beta\gamma \;\; z_p^2 \;\; RD(\alpha^2+\lambda, \beta^2+\lambda, \gamma^2+\lambda)$$

$$V_4 = -3\alpha\beta\gamma \;\; RF(\alpha^2+\lambda, \beta^2+\lambda, \gamma^2+\lambda)$$

Here the parameters to the functions are given such that, in terms of variable $t^{'} = t + \lambda$, the limits of integral become λ to ∞. Finally to get the scaled up value of potential,

$$U(\mathbf{r}) = \pi G\sigma L^2(V_1 + V_2 + V_3 + V_4)$$

Refer to [22] for further details.

2.2 2D approximation

For 2D analysis, we give appropriate values of α and β and a small value of γ. While calculating accelerations on particles we use a **Central Difference Scheme** to obtain spatial gradients of the potential.

$$a_x = \frac{U(x+\Delta x, y, z) - U(x-\Delta x, y, z)}{2\Delta x}$$

Similarly, for a_y and a_z. We give initial conditions such that, the z-coordinate of all particles free to move is zero, making the analysis 2D. As a result and owing to the symmetry of the gravitational potential about $x-y$ plane, the *particles experience no force in the z-direction*, keeping their motion restricted to the same plane, only. Note that, the gravitational potential is also symmetric about $x-z$ and $y-z$ planes and hence the few particles lying on them would not experience any acceleration in the y and z directions respectively.

Coriolis and centrifugal acceleration:

The ellipse rotates about the z-axis with angular velocity ω_{cb} in the counter-clockwise direction. In the frame of the ellipse,

$$\mathbf{a} = \frac{F}{m} - 2(\omega_{cb} \times \mathbf{v}) - \dot{\omega_{cb}} \times \mathbf{r} - \omega_{cb} \times (\omega_{cb} \times \mathbf{r})$$

where $\mathbf{a}$ and $\mathbf{v}$ are the acceleration and velocity of a particle respectively. Since $\dot{\omega_{cb}}$ is zero, in x and y direction accelerations boil down to,

$$a_x = g_x + 2\omega_{cb}v_y + \omega_{cb}^2 x$$

$$a_y = g_y - 2\omega_{cb}v_x + \omega_{cb}^2 y$$

2.3 Parameters and initial conditions

We have modified an a classical molecular dynamics code called LAMMPS (acronym for Large-scale Atomic/Molecular Massively Parallel Simulator) make by Steve Plimpton [21]. It is open-source and has a 'GRANULAR' package for *grains* that uses SSDEM (Soft Sphere Discrete Element Method). Note that the word *grains*, henceforth, refers to frictional elastic spheres of constant density. The simulation domain is 3D in reality but 2D in essence, as we have kept the flow restricted to the equatorial plane of a flattened ellipsoid. The boundary is lined with grains fixed in space and the equations are solved in a rotating frame of reference. The collisions are modelled using a set of tangential and normal springs and dampers. When the distance r between two particles of radii R_i and R_j is less than their contact distance $d = R_i + R_j$ the spring and dampers are activated. There is no force between the particles when $r>d$.
The Hookean contact styles use this formula:

$$F_{hk} = \Big(k_n \delta n_{ij} - m_{eff}\gamma_n v_n\Big) - \Big(k_t \Delta s_t + m_{eff}\gamma_t v_t\Big)$$

The Hertzian style uses this formula:

$$F_{hz} = \sqrt{\delta}\sqrt{\frac{R_i R_j}{R_i + R_j}}F_{hk} = \sqrt{\delta}\sqrt{\frac{R_i R_j}{R_i + R_j}}\Big(k_n \delta n_{ij} - m_{eff}\gamma_n v_n\Big) - \Big(k_t \Delta s_t + m_{eff}\gamma_t v_t\Big)$$

$\delta = d - r$	overlap distance of 2 particles
K_n	elastic constant for normal contact
K_t	elastic constant for tangential contact
γ_n	viscoelastic damping constant for normal contact
γ_t	viscoelastic damping constant for tangential contact
$m_{eff} = M_i M_j/(M_i + M_j)$	effective mass of 2 particles of mass M_i and M_j
n_{ij}	unit vector along the line connecting the centers of the 2 particles
V_n	normal component of the relative velocity of the 2 particles
V_t	tangential component of the relative velocity of the 2 particles

Table 1: Definitions of terms used

The first parenthesized term is the normal force between the two particles and the second parenthesized term is the tangential force. The normal force has 2 terms, a contact force and a damping force. The tangential force also has 2 terms, a shear force and a damping force. The shear force is a "history" effect that accounts for the tangential displacement between the particles for the duration of the time they are in contact. The exact details of the simulations are given below.

Number of flowing particles	24248
Diameter of flowing particles	$1m$
Diameter of basal particles	$21m$
Density of elliptical core	$2 \times 10^5 kgm^{-3}$
Density of particles	$1500 kgm^{-3}$
a	$1000m$
μ	0.4
Semi-minor axis	$10m$
Coefficient of restitution	1
Timestep	$0.396s$
Stiffness of tangential spring	$7000 Nm^{-1}$
Stiffness of normal spring	$10000 Nm^{-1}$
Damping of tangential and normal dashpots	$0 Nsm^{-1}$
Direction of rotation	anti-clockwise

Table 2: Details of simulations

The density of the core is taken such that the accelerations produced at the surface is of the order $1mms^2$, as is true for as asteroids like Itokawa [17]. We have considered the following initial conditions. A layer of constant depth all over the surface. Such conditions may arise from alternate heating and cooling of the asteroid surface, resulting in crack formation and finally failure to form loose regolith. This is called thermal fragmentation [17]. All particles are initialised with a data file created externally. The procedure for generating coordinates of all particles for the specific initial conditions is outlined below.

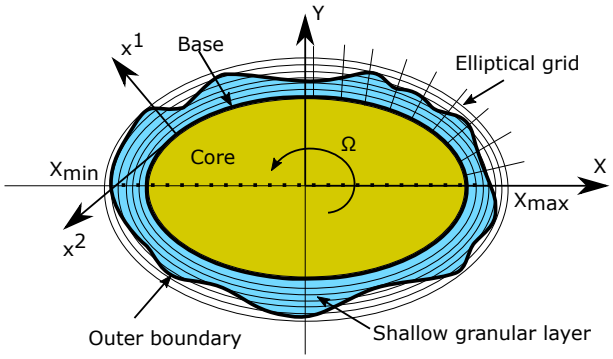

Figure 1: Schematic for the problem

- Obtain X_{max} and X_{min} as in figure 1.
- Define diameter of flowing particles and split the distance between X_{max} and X_{min} into parts such that each is one diameter in length.
- For every abscissa obtained thus, ν is obtained using $x = acosh(\mu)cos(\nu)$.
- Ordinate for the base is obtained using max of 0 or y, as solved from the equation of the ellipse $x^2/a^2 + y^2/b^2 = 1$.
- The outer boundary ordinate is obtained using $y = asinh(\mu + d\mu)sin(\nu)$, where $d\mu = height/\sqrt{g}$ and $g = (sinh(\mu))^2 + (sin(\nu))^2$.
- For every particle assigned between the base and the outer boundary above the X-axis (+) and one is assigned below(-).
- The *height* above the base is defined as constant or Gaussian (for hill break).

2.4 Post processing

- We define an elliptical grid starting from ν equals 0 to 2π, with nodes at different heights(μ) for each ν.
- Coordinates of all particles are mapped on to this grid.
- The closest point on the grid is sought by scanning the abscissa of a particle first, followed by a scan for those ν which are in the neighborhood of the ordinate corresponding to the abscissa obtained previously, along different μ i.e. height.
- Particles without any form of energy dissipation (friction), bounce too much, such that concentration of particles decreases in certain regions. Also, during mass shedding, chunks of particle aggregates get detached from the base. This results in an apparent increase in volume of flow and causes difficulty in calculating the real height of flow.
- A matrix called *weight*, stores the multiplicity of mapped points for each node on the grid.
- For every ν, the height till which continuum holds is that before which *weight* is zero for the first time, while travelling in the outward radial direction. In figure 2 we see that weight becomes zero at $7.5m$ for the first time, after which material is detached from the base.

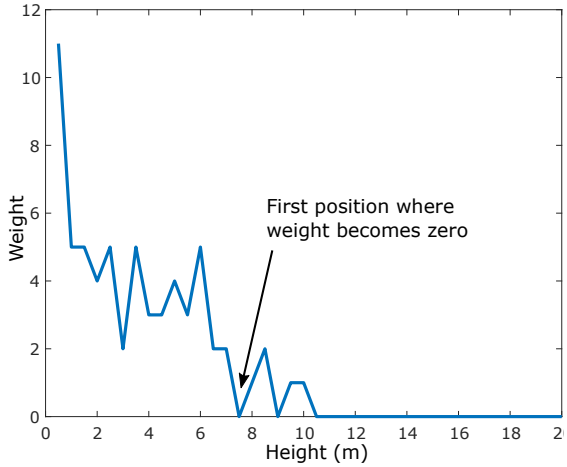

Figure 2: Weight distribution in radial direction

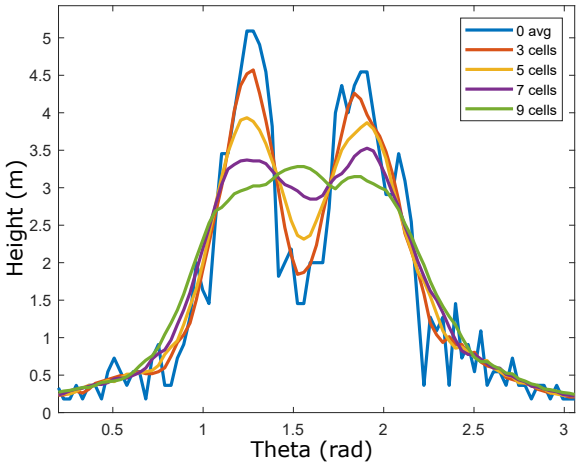

Figure 3: Effect of averaging on smoothness

- We apply a certain averaging in tangential direction.
- The quality of averaging for smoothness affects the overall quality of data and we can see that the nature of the plot (see figure 3) entirely changes for averaging with greater number of cells.
- An optimum cell number is selected for averaging.

3 Results and discussion

First we try to make an estimate of the range of angular velocities that may show interesting physics. For non-rotating, homogeneous tri-axial ellipsoids the gravitational potential on the surface is lowest at the ends of its short axis, and highest at the ends of its long axis. However, the surface gravity shows the exact opposite behaviour [18]. On introducing rotation, centrifugal forces compete with gravitational, to redistribute mass over the surface. On increasing Ω for

zero angle of friction, we may identify two critical angular velocities. The first, corresponding to change of direction of migration from minor to major axis, and the second, corresponding to shedding of stationary mass from major axis.

3.1 Choice of angular velocities

In figure 4, we see the variation of the absolute value of effective acceleration *i.e.* difference between centrifugal and gravitational acceleration at the end of the major (blue) and minor (red) axes of the ellipse. Mass shedding starts from the major axis beyond $\Omega = 0.9 rads^{-1}$ as centrifugal force overpowers gravitation here. Beyond $\Omega = 1.9 \times 10^{-3} rads^{-1}$ mass shedding happens everywhere. It is to be noted that, *these values are true for a stationary particle on the surface, and not for ones that have finite velocity in either direction tangential to the surface.* Thus, we conclude that reshaping would occur without shedding, only for values of Ω lesser that $0.9 \times 10^{-3} rads^{-1}$, not larger. For real asteroids having length of the order of hundred meters, critical shedding Ω, has been observed to be $\sim 0.75 \times 10^{-3} rads^{-1}$ (Pravec *et. al.* (2007)) [23], which is close to the values obtained here.

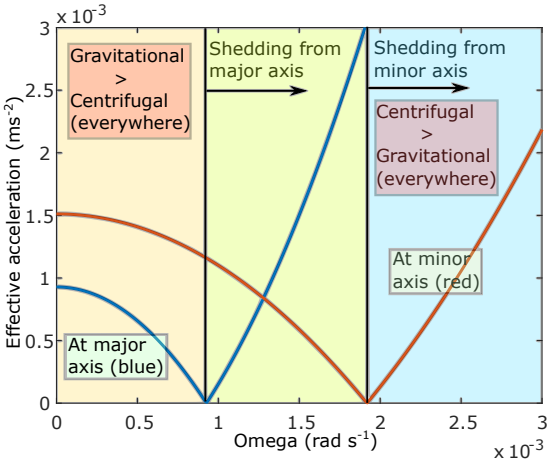

Figure 4: Ω for mass shedding

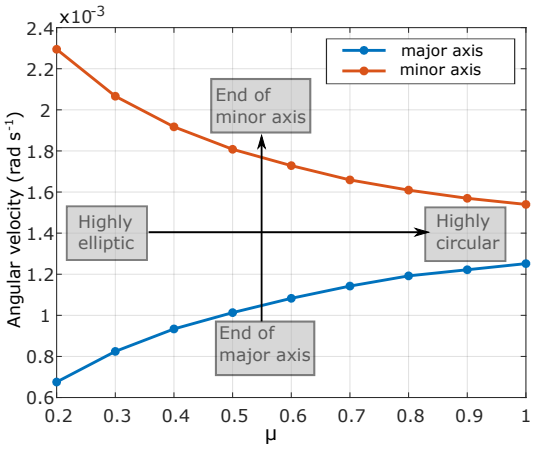

Figure 5: Shedding Ω for different eccentricities

In figure 5 we see the effect of eccentricity on the critical angular velocity for shedding (let's say *critshed*). As eccentricity decreases, for a constant area of the ellipse, the geometry becomes more circular, causing the *critshed* at the end of minor and major axis to decrease and increase respectively, finally merging to the same value for a circle. Due to the lack of tangential forces on a circle, flow on it's surface is not likely to happen before mass is directly shed from all points. We may say, that for similarly sized bodies rotating with similar angular velocity, regolith cover is likely to be thicker for spherical geometries than elliptic. This is because, the tangential component of the net force for elliptic bodies (much fainter for spherical ones) causes surface motion, effectively reducing the shedding Ω.

3.2 Effect of friction

For any flow to start from rest at some point on the surface, basal friction must be overcome by the tangential component of net force at that point (see figure 6). It may so happen that moving material, pushes the otherwise stationary, leading to change of topography in unexpected regions. For example, craters are gravitationally stable regions with little movement. However, over longer periods of time they appear to become shallow owing to regolith motion from higher gravitational potentials. Evidences of crater degradation has been observed on asteroid Vesta, as reported by Vincent *et al.* in 2013 [25].

When there is no friction, there exists only one value of Ω, for which tangential force becomes zero at every point. This is the first critical Ω as stated in the beginning of this section.

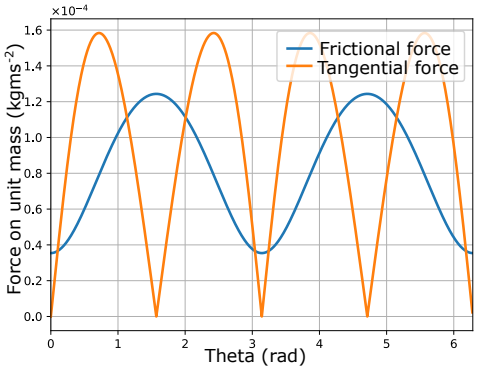

Figure 6: Typical distribution of forces

For higher coefficients of friction, there is a range of angular velocities for which the blue curve is above the orange one. These correspond to no movement. In figure 7, we show the different combinations of friction and angular velocities that may or may not cause movement in different directions for $\mu = 0.2$. At lower angular velocities, gravity dominates and mass moves towards the minor axis much like landslides on the Earth. Beyond the upper bound of the critical region of no movement, migration is observed towards the major axis.

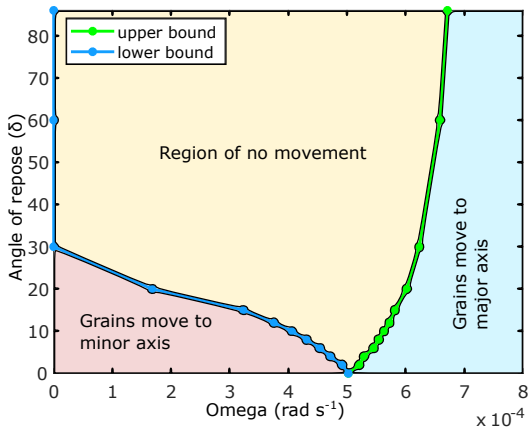

Figure 7: Different regimes of movement

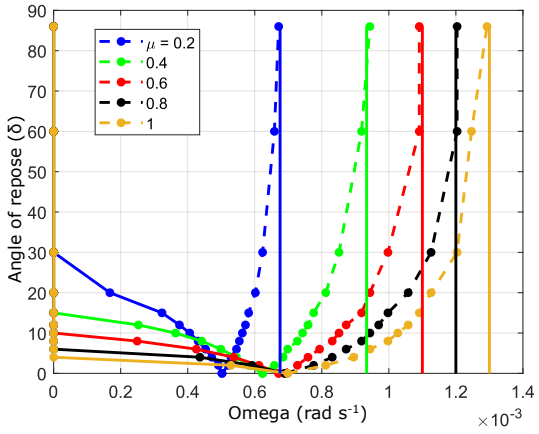

Figure 8: Critical regime for different eccentricities

Figure 8 shows the critical region for different eccentricities of the ellipse considered, such that mass is the same for all cases. The dotted and solid lines represent the upper and lower bounds respectively (refer to figure 7). The solid vertical lines represent shedding Ω the major axis for each eccentricity. At higher angles of repose, we see the upper bound increasing to meet that of shedding Ω *i.e. critshed*. This is because, dramatically high friction causes the regolith layer to be almost rigid (in theory), which implies that mass has already been shed from the surface. We see that the region of no movement grows larger in size with the increase in μ *i.e.* with decrease in eccentricity. This is again because, the tangential component of net force is almost zero for nearly circular geometries. With decrease in eccentricity, tangential forces decrease at all angular positions (higher values of μ in figure 10), resulting in a larger window of angular velocities for which there is no movement. However, the normal part which is always negative, unless rotation is strong enough, does not increase definitively at all locations on the ellipse. Figure 9 shows an increasing frictional force at 0^o and 30^o and a decreasing one at 60^o and 90^o.

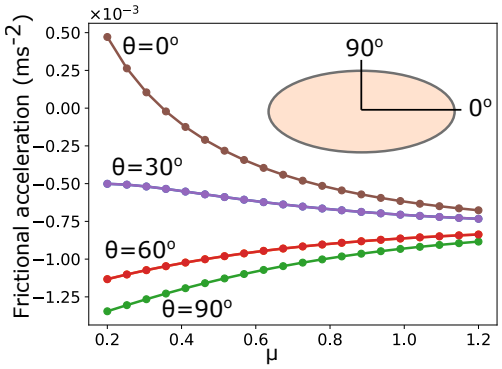

Figure 9: Variation of frictional acceleration

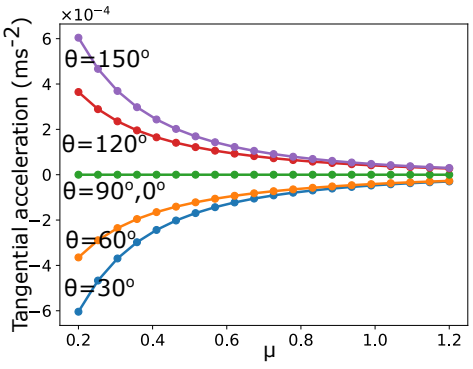

Figure 10: Variation of tangential acceleration

Through post-processing we find out height distribution profiles for steady state conditions *i.e.* after equilibriation. Equilibriation time is basically a measure of time required for all forces on the particles to get equilibriated in a situation of zero velocity. The Kinetic Energy (KE) of the particles in the rotating frame of reference, does not go to an exact zero, as it ideally should, so we set a threshold value ($10^{-1} joule$), beyond which it is considered to be too small to represent significant movement. Figure 11 shows the relationship between equilibriation time and coefficient of friction. We see that, as the coefficient of friction increases, dissipation increases and thus the system is equilibriated quickly. Thus, any observed dynamical phenomena on the surface, may signify the following. It may be the aftermath of short-termed exogenic events, like impacts or slope failures, that had only recently occurred. It may also mean, that long-termed endogenic processes like faulting, tectonic shifts or volcanic activities, that effectively lower the coefficient of friction of regolith, are still going on. There could also be long-term causes like YORP or tidal torque that result in sudden surface motion due to rotational instability. These reasons are outlined in Mudroch *et al.* (2015) [17]. Note that we ignore the KE of mass that has been shed.

3.3 Some definitions

For the parameters stated in section 2.3, figure 12 shows the steady state distribution of height from 0 to 2π, for two typical cases of rotation, below and beyond the region of no movement (refer to figure 7) that is responsible for the change in direction of migration. We refer to the movement of mass towards the minor and major axes as *Pre-critical* and *Post-critical* regimes.

Certain angular velocities cause the core of the asteroid to get exposed due to surface shedding [16]. Here, we estimate exposure through the term *spread*. At low rotation rates mass migrates towards the minor axis leaving the major axis vacant. At higher ones, mass is shed from the major axis, resulting in a similar phenomena provided friction is high enough to allow the mass at minor to remain unperturbed. Thus, we may ask the question, does exposure occur before or after mass shedding?

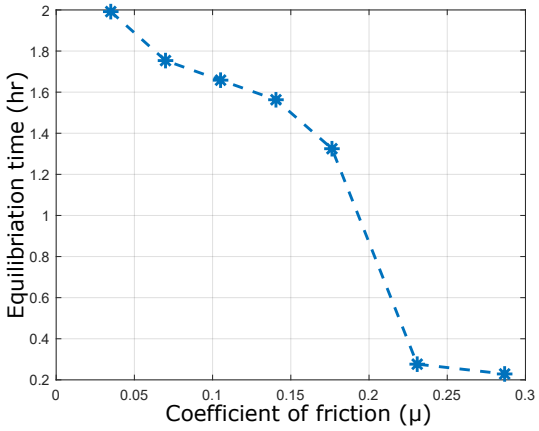

Figure 11: Equilibriation time

3.4 Pre-critical regime (DEM)

This regime is characterised by low rotation rates, such that mass migrates towards the end of minor axis under the dominating influence of gravity. The flow remains symmetric about both X and Y axes at all times, when rotation is absent. Because of this, the maximum height is calculated by taking an average of the maximum height in each quadrant *i.e.*,

$$height = \frac{h^1 + h^2 + h^3 + h^4}{4}$$

However, on introducing rotation, asymmetries form, because of which there are two different maximas. The first and third quadrants are symmetric and so are the second and fourth. The maximum heights are then defined as,

$$height^1 = \frac{h^1 + h^3}{2} \quad and \quad height^2 = \frac{h^2 + h^4}{2}$$

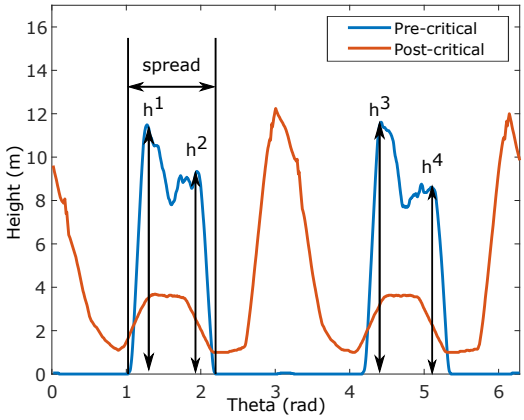

Figure 12: Typical height distribution for two different cases. Blue: $\omega = 3 \times 10^{-4}$. Red: $\omega = 3 \times 10^{-4}$. Angle of friction for both is 4°

The reason for this asymmetry is the Coriolis acceleration ($Coriolis = -\Omega \times v$). The gravitational and centrifugal accelerations are negative and positive respectively in all quadrants as they are dependent only on position of the particle. However, the Coriolis component depends on velocity. Several asymmetric surface phenomena have been described by Burns and Dobrovolskis in 1980 [27]. If the direction of movement of a particle is prograde (along the positive tangential

direction) then the Coriolis is directed outwards from the ellipse. For retrograde motion (along the negative tangential direction), it is directed inwards. The magnitude of this force is very small in the *Pre-critical* regime, as Ω is very small. In figure 12, h_1 is slightly greater than h_2, as velocity is retrograde in the second quadrant resulting in the suppression of the hill formed. In this case, although it's effect on the height of hills formed is noticeable, trends due to increase in Ω and coefficient of friction are not. This is because, both hinder regolith movement in the *Pre-critical* regime, as can be seen in the following paragraph, resulting in lower velocities and thus lesser asymmetries.

The following graph (figure 13) shows how maximum height (*i.e.* $height^2$) decreases with coefficient of friction, as friction dissipates all the kinetic energy acquired by the particles due to gravitational acceleration. The starting profile is has a uniform height of approximately $4m$ all through. For higher coefficients of friction we see that the maximum height is close to the starting height, meaning that there has been very little redistribution of matter.

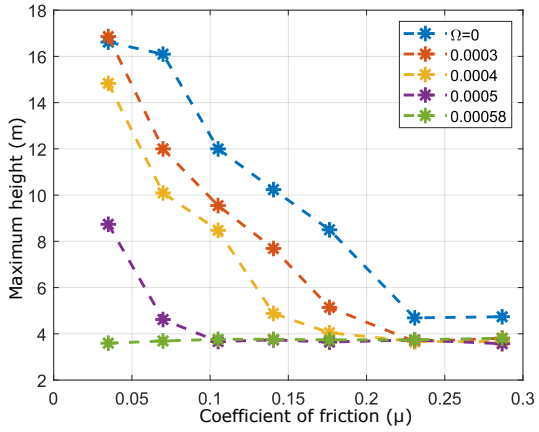

Figure 13: Maximum height

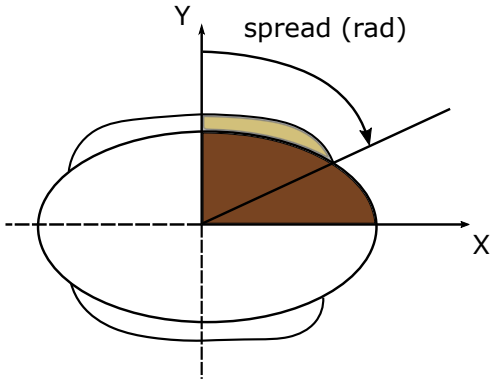

Figure 14: Schematic for spread

With an increase in Ω, the maximum height decreases due to a balance of the two competing primary forces. This signifies that in the *Pre-critical* regime, superficial irregularities due to loose regolith are less probable to occur for higher angular velocities. However, in the *Post-critical* regime, but before mass shedding, the reverse is likely to occur (we see later). This is because the centrifugal force causes hill formation at the ends of the major axes.

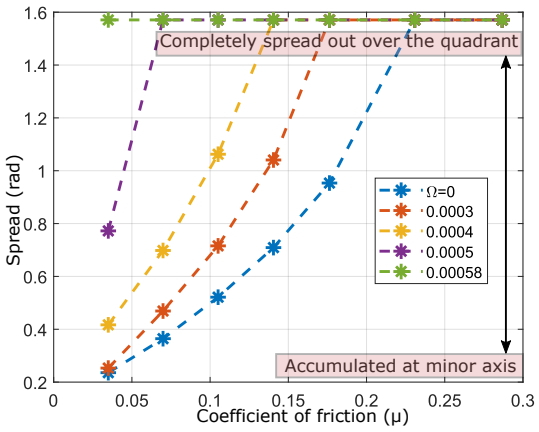

Figure 15: Spread

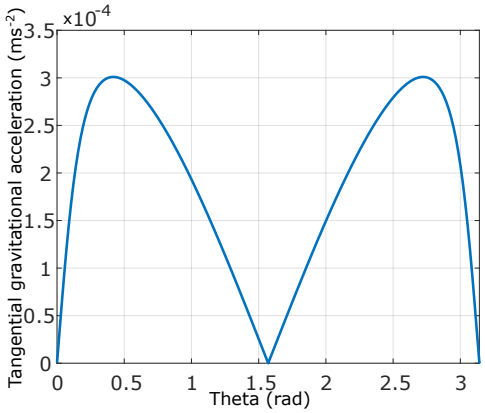

Figure 16: Tangential acceleration at the surface of an ellipse

In steady state, the region on the ellipse that is covered with grains is termed as *spread*, as shown in figure 14 and figure 12. Due to almost negligible asymmetry, we have considered the

spread in the first quadrant only. Increasing friction and rotation have similar effects on *spread*. For relatively smooth basal topographies, exposure (complement of *spread*) is maximum for slow rotators at low coefficients of friction at the ends of the major axis.

A surface may be defined as steep or flat based on whether the magnitude of tangential forces acting on it are high or low. Figure 10 shows that the magnitude of tangential forces at 30° is higher than that at 60°. In fact, the magnitude spikes up from zero near the ends of the major axis and slowly goes back down at the end of minor axis (see figure 16). Thus, the neighbourhood of the major axis may be called steep. Saito *et al.* (2006) [28] talks about the exposed surfaces on the asteroid Itokawa occurring in steep topographies. Figure 15 shows the variation of *spread* with μ. Material is seen to move towards the minor axis, exposing the underlying surface of the core at the major axis, which is really the steep region.

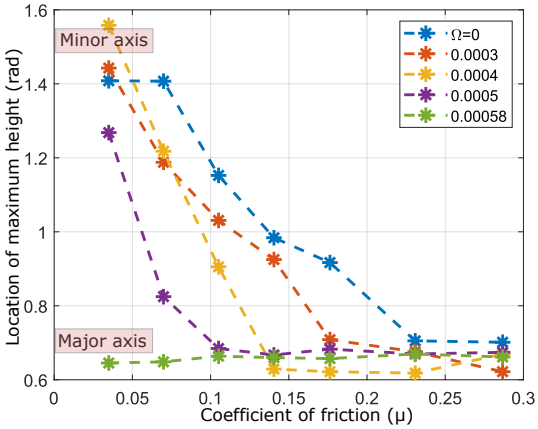

Figure 17: Location of maximum height

From figure 17 we can see that that the location of maximum height shifts from the minor to the major axis as it decreases in value with increase in coefficient of friction. In reality, granular deposits at gravitational highs have been thought to result from downslope movements. This is backed by observations that suggest, halting of loose regolith due to frictional or other effects before reaching the foot of the slope in Mantz *et al.* (2004) [24]. Flowing debris has not gained it's lowest potential due to friction. For higher rotation rates there is little movement, resulting in a small peak near the end of major axis.

3.5 Post-critical regime (DEM)

The post critical regime is characterised by higher rotation rates that cause mass migration towards the major axis leading to shedding. The height at the end of major axis is observed to increase with rotation. However, as the angular velocities increase mass shedding takes place and the height decreases. At lower coefficients of friction, the material is more fluid-like and mass shedding happens for lower values of Ω. As the height goes to zero, for high Ω, we see that the major axis is exposed once again.

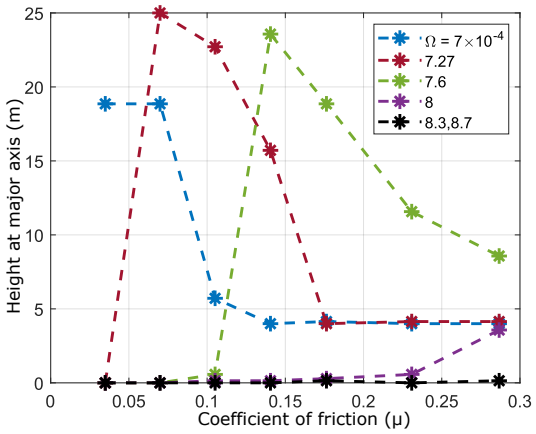

Figure 18: Height at the major axis

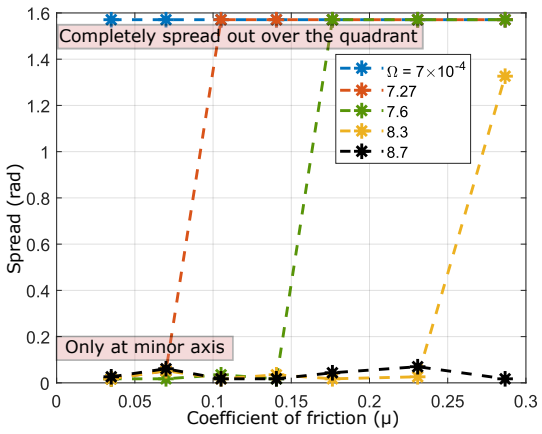

Figure 19: Spread

Here, in figure 19, we see that the *spread* varies rather drastically with coefficient of friction. This exposure is post mass shedding. For every coefficient of friction there is a certain angular velocity till which the surface remains completely covered, after which almost all of the material is shed from the ellipse. It signifies that, for relatively fast rotators, once shedding starts, a significant amount of material is shed, such that they tend to have a majority of exposed surfaces (which is kind of obvious). Thus, the surface of asteroids can change drastically, in terms of regolith cover, even from slow spin up due to YORP beyond some critical angular velocity, in this regime. This is commensurate with [16], where Scheeres states that asteroid surfaces are bound to change their shape over their lifetimes.

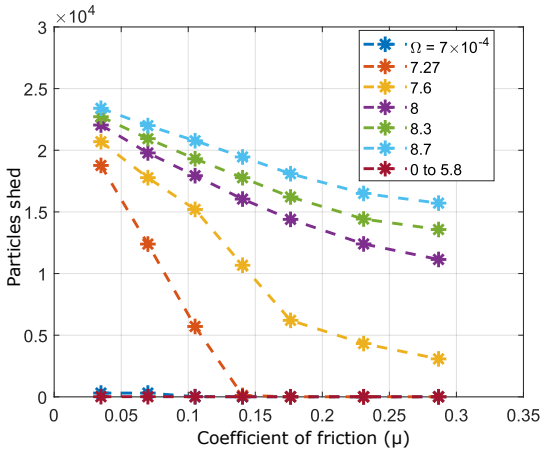

Figure 20: Mass shedding

4 Conclusions

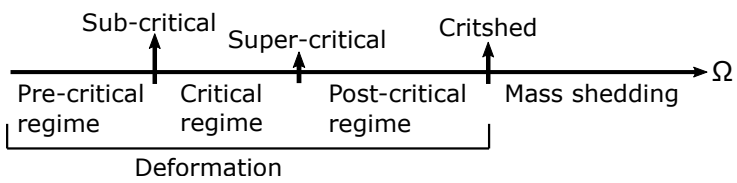

Figure 21: Separate regimes

In conclusion, we can say that some regimes have been identified as the angular velocity is increased. The first is where, gravity dominates centrifugal forces and is primarily responsible

for the associated shape changes. We call this as the *Pre-critical* regime. The *Sub-critical* Ω marks the end of this regime and this is followed by the *Critical regime*, where centrifugal and gravitational forces slowly come to a balance, resulting in very little movement of surface material. With an increase in the angle of friction, the width of this regime increases. As the centrifugal forces start overcoming gravitation, we move into a regime, we call *Post-critical*, starting from *Super-critical* Ω. So far the asteroid surface only deforms to a new shape under different forces. Beyond *critshed* there is loss of mass from the surface due to strong centrifuging. Mass shedding increases with Ω until the entire ellipse is exposed. Refer to figure 21. [16] talks about a similar classification for completely granular aggregates.

This is broadly followed just at the surface of the ellipse for material that is stationary. The height of the layer of grains, or any finite velocity is not considered, while deriving the bounds of the regimes. However, a shallow layer approximately adheres to such classification, with minor deviations. This is why, we may find slight movement even for certain angular velocities in the *Critical* regime.

Mass shedding is an important, *Post-critical* phenomenon. However, exposure of core is not a consequence of just that. We find that exposure can happen in two cases. First, for very slow rotators, where gravitation drives flows from higher elevations to minimize potential energy, leaving them exposed. This is similar to landslides happening on the Earth. Second, when the angular velocity is too high for mass to escape from the surface, leading to exposure. In both cases the ends of the major axis is exposed. However, in the second case, exposure from spin up is rather sudden than gradual, as is true for the first.

References

[1] Chandrasekhar, S. *Ellipsoidal figures of Equilibrium.* Yale University Press (1969).

[2] Darwin, G. H. *On the Figure and Stability of a Liquid Satellite.* Philosophical Transactions of the Royal Society of London, Vol. 206 (1906), pp. 161-248.

[3] Sharma, I. *Equilibrium shapes of rubble-pile binaries: The Darwin ellipsoids for gravitationally held granular aggregates.* Icarus 205 (2010) 638–657.

[4] Sharma, I. *Structural integrity of rubble asteroidal satellites.* Icarus 319 (2019) 770–784.

[5] Aggarwal, H.R., Oberbeck, V.R. *Roche limit of a solid body.* Astrophysical Journal 191 (1974) 577–588.

[6] Dobrovolskis, A.R. *Internal stresses in Phobos and other triaxial bodies.* Icarus 52 (1982) 136–148

[7] Davidsson, B. *Tidal splitting and rotational breakup of solid biaxial ellipsoids.* Icarus 149 (2001) 375–383.

[8] Chauvineau, B., Farinella, P. and Mignard, F *Planar orbits about a triaxial body: applications to asteroidal satellites.* Icarus 105 (1993) 370–384.

[9] Scheeres, D.J. *Dynamics about uniformly rotating triaxial ellipsoids: application to asteroids.* Icarus 110 (1994) 225–238.

[10] Guibout, V., Scheeres, D.J. *Stability of surface motion on a rotating ellipsoid.* Celest. Mech. Dyn. Astron. 87 (2003) 263–290

[11] Kevin J. Walsh, Derek C. Richardson,Patrick Michel *Rotational breakup as the origin of small binary asteroids.* Nature, 454 (2008) 188

[12] Sanchez P. D., Scheeres, D.J. *DEM simulation of rotation-induced reshaping and disruption of rubble-pile asteroids.* Icarus 218 (2012) 876-894

[13] Walsh K. J., Richardson D. C., Michel P. *Spin-up of rubble-pile asteroids: Disruption, satellite formation, and equilibrium shapes.* Icarus 220 (2012) 514-529

[14] Hirabayashi M. *Structural failure of two-density-layer cohesionless biaxial ellipsoids.* Icarus 236 (2014) 178-180

[15] Hirabayashi M., Scheeres D.J. *Stress and failure analysis of rapidly rotating asteroid (29075) 1950 DA.* The Astrophysical Journal Letters 798 (2015) L8

[16] Hirabayashi M., Sanchez P. D., Scheeres D.J. *Internal Structure of Asteroids Having Surface Shedding due to Rotational Instability.* The Astrophysical Journal 808 (2015) 63

[17] Naomi Murdoch, Sanchez P. D., Stephen R. Schwartz, Hideaki Miyamoto *Asteroid Surface Geophysics.* arXiv:1503.01931v1 (2015)

[18] Anthony R. Dobrovolskis *Classification of Ellipsoids by Shape and Surface Gravity.* Icarus 321 (2019) 891-928

[19] Hideaki Miyamoto *et. al. Migration and Sorting on Asteroid Itokawa.* Science 316, 5827 (2007) 1011-1014

[20] D. S. Lauretta, D. N. DellaGiustina *et. al. The unexpected surface of asteroid (101955) Bennu.* Nature 568 (2019) 55–60

[21] Steve Plimpton *Fast Parallel Algorithms for Short–Range Molecular Dynamics.* Journal of Computational Physics 117 (1995) 1-19

[22] Scheeres D.J. *Orbital Motion in Strongly Perturbed Environments: Applications to Asteroid, Comet and Planetary Satellite Orbiters.* Springer ISBN-13: 978-3642032554 (2012)

[23] Pravec Petr, Harris A. W., Warner B. D. *Near Earth Objects, our Celestial Neighbors: Opportunity and Risk.* Proceedings if IAU Symposium 236 (2007) 167-176

[24] A. Mantz, R. Sullivan, J. Veverka *Regolith transport in craters on Eros.* Icarus 167 (2004) 197-203

[25] J.-B. Vincent *et al. Crater depth-to-diameter distribution and surface properties of (4) Vesta.* Planetary and Space Science 103 (2014) 57-65

[26] Krohn K. *et al. Mass movement on Vesta at steep scarps and crater rims.* Icarus 244 (2014) 120-132

[27] Dobrovolskis A. R., Burns J. A. *Life near the Roche Limit: Behavior of Ejecta from Satellites Close to Planets.* Icarus 42 (1980) 422-441

[28] Saito J. *et al. Detailed images of asteroid 25143 Itokawa from Hayabusa.* Science 312, 5778 (2006) 1341-1344